

Modified Zimányi-Moszkowski model for finite nuclei

Guo Hua,¹ Y. X. Liu,^{1,2} and S. Yang¹

¹*Department of Technical Physics and MOE Key Laboratory of Heavy Ion Physics, Peking University, Beijing 100871, People's Republic of China*

²*Department of Physics, Peking University, Beijing 100871, People's Republic of China*

(Received 31 May 2000; published 21 March 2001)

A modified Zimányi-Moszkowski model for finite nuclei is investigated in this paper. The improvement on the Zimányi-Moszkowski (ZM) model is achieved by including a tensor force. It shows that in the ZM model the spin-orbit splittings of finite nuclei can be improved by the inclusion of a tensor coupling. Furthermore, the tensor force is generally attractive in the interior of nuclei and repulsive in the surface region. As a result, nucleons become more tightly bound in the deep-lying states, and more loosely bound in the states close to the Fermi surface, when the tensor force is included.

DOI: 10.1103/PhysRevC.63.044320

PACS number(s): 21.60.-n, 21.10.-k, 21.30.Fe

I. INTRODUCTION

The Zimányi-Moszkowski (ZM) model [1] is useful in explaining many experimental properties of nuclear matter in the mean field approximation (MFA). This model gives a reasonable incompressibility for nuclear matter ($K_v \approx 225$ MeV), and a large effective nucleon mass ($M^*/M \approx 0.85$ MeV) [2,3]. Furthermore, the ZM model can be considered as an extended version of the linear Walecka model [4], in which the scalar coupling constant becomes effectively related to the nuclear matter density through the σ -meson field. This density dependent coupling is useful in the description of heavy-ion collisions [5]. On the other hand, the spin-orbit splittings are known to be the important properties of finite nuclei. As pointed out in Refs. [6,7], the spin-orbit splittings for finite nuclei given by the ZM model are too small compared with the experimental findings. The reason for this shortcoming is that the effective nucleon mass at saturation density given by the ZM model is large, and results in small spin-orbit splittings due to the weak mean fields [6,7]. In order to overcome this shortcoming, Biró and Zimányi have recently proposed a new effective Lagrangian, in which a tensor coupling term is introduced [referred to as the modified Zimányi-Moszkowski (MZM) model] [8]. The positive features of the MZM model are that the good properties of the ZM model for nuclear matter are unchanged, while the spin-orbit potential is expected to be improved. Recent investigations have also shown that the inclusion of a tensor coupling term to the ZM Lagrangian does not change the thermodynamic properties of nuclear matter in the MFA [9], and can obtain the reasonable behaviors of the temperature and density dependence of the ρ -meson mass [10]. It has also been shown that the tensor coupling in the MZM model is especially helpful in describing the spin-orbit splittings [11]. Nevertheless, the MZM model proposed by Biró and Zimányi has not been used to describe the properties of finite nuclei; what role the tensor force plays, and how the tensor coupling affects the single particle spectrum in the MZM model remain unclear. In this paper, we extend the MZM model investigations to the study of finite nuclei, and attempt to shed light on the role the tensor coupling plays in the MZM model for finite nuclei.

The paper contains four sections. In Sec. II we will review the MZM model and derive some basic formulas for finite nuclei. In Sec. III we will present numerical results and discussions. The paper gives our conclusion in Sec. IV.

II. THE MZM MODEL

The extended Lagrangian for the MZM model is given by

$$\begin{aligned} \mathcal{L} = & \bar{\psi} \left\{ \gamma_\mu \left[i \partial^\mu - e \frac{1 + \tau_3}{2} A^\mu \right] - g_\omega \omega^\mu - g_\rho \vec{\tau} \cdot \vec{b}^\mu \right\} \\ & - M^* - \frac{f_v}{4M^*} g_\omega \sigma^{\mu\nu} F_{\mu\nu} \left\} \psi + \frac{1}{2} (\partial_\mu \phi \partial^\mu \phi - m_\sigma^2 \phi^2) \\ & + \frac{1}{2} m_\omega^2 \omega_\mu \omega^\mu - \frac{1}{4} F_{\mu\nu} F^{\mu\nu} + \frac{1}{2} m_\rho^2 \vec{b}_\mu \cdot \vec{b}^\mu - \frac{1}{4} \vec{G}_{\mu\nu} \cdot \vec{G}^{\mu\nu} \\ & - \frac{1}{4} A_{\mu\nu} A^{\mu\nu}, \end{aligned} \quad (1)$$

where the tensor coupling of the ω -meson field to the nucleon field is included, f_v stands for the tensor coupling constant, and ϕ the σ -meson field. We also use the following notations, $F_{\mu\nu} \equiv \partial_\mu \omega_\nu - \partial_\nu \omega_\mu$, in which ω_μ is the ω -meson field, $\vec{G}_{\mu\nu} \equiv \partial_\mu \vec{b}_\nu - \partial_\nu \vec{b}_\mu$, with the isovector field \vec{b}_μ , $A_{\mu\nu} \equiv \partial_\mu A_\nu - \partial_\nu A_\mu$, and $\sigma_{\mu\nu} \equiv (i/2)[\gamma_\mu, \gamma_\nu]$. If $f_v = 0$, the MZM model goes back to the ZM model. It is remarkable that the term of tensor coupling in the MZM model contains a nonlinear coupling between the σ - and ω -meson fields due to the effective nucleon mass M^* :

$$M^* = M - m^* g_\sigma \phi, \quad (2)$$

in which the parameter m^* is given by

$$m^* = \frac{1}{1 + \frac{g_\sigma \phi}{M}}. \quad (3)$$

With Eq. (1), the equations of motion for finite nuclei can be derived in the MFA as

TABLE I. Coupling constants C_i^2 with the definitions $C_i^2 \equiv g_i^2(M/m_i)^2$ ($i = \sigma, \omega, \rho$) for the MZM model. The mass parameters M , m_σ , and m_ρ are given in units of MeV.

C_σ^2	C_ω^2	C_ρ^2	M	m_σ	m_ω	m_ρ
177.396	63.478	29.550	938.27	525	783	770

$$\begin{aligned} & \frac{d^2}{dr^2} \phi(r) + \frac{2}{r} \frac{d}{dr} \phi(r) - m_\sigma^2 \phi(r) \\ &= -g_\sigma m^{*2}(r) \rho_s(r) + \frac{f_v g_\sigma g_\omega}{2M^2} \frac{d\omega_0(r)}{dr} \rho_t(r), \end{aligned} \quad (4)$$

$$\begin{aligned} & \frac{d^2}{dr^2} \omega_0(r) + \frac{2}{r} \frac{d}{dr} \omega_0(r) - m_\omega^2 \omega_0(r) \\ &= -g_\omega \left[\rho(r) + \frac{f_v}{2M^*(r)} \frac{d}{dr} \rho_t(r) + \frac{f_v g_\sigma}{2M^2} \frac{d\phi(r)}{dr} \rho_t(r) \right], \end{aligned} \quad (5)$$

$$\frac{d^2}{dr^2} b_0(r) + \frac{2}{r} \frac{d}{dr} b_0(r) - m_\rho^2 b_0(r) = -g_\rho \rho_3(r), \quad (6)$$

$$\frac{d^2}{dr^2} A_0(r) + \frac{2}{r} \frac{d}{dr} A_0(r) = -e \rho_p(r), \quad (7)$$

where

$$\rho(r) = \sum_\alpha \frac{2j_\alpha + 1}{4\pi r^2} (|G_\alpha(r)|^2 + |F_\alpha(r)|^2), \quad (8)$$

$$\rho_s(r) = \sum_\alpha \frac{2j_\alpha + 1}{4\pi r^2} (|G_\alpha(r)|^2 - |F_\alpha(r)|^2), \quad (9)$$

$$\rho_3(r) = \sum_\alpha \frac{2j_\alpha + 1}{4\pi r^2} (-1)^{(\tau_\alpha - 1)/2} (|G_\alpha(r)|^2 + |F_\alpha(r)|^2), \quad (10)$$

$$\rho_p(r) = \sum_\alpha \frac{2j_\alpha + 1}{4\pi r^2} \left(\frac{\tau_\alpha + 1}{2} \right) (|G_\alpha(r)|^2 + |F_\alpha(r)|^2), \quad (11)$$

$$\rho_t(r) = \sum_\alpha \frac{2j_\alpha + 1}{4\pi r^2} 2G_\alpha(r)F_\alpha(r), \quad (12)$$

and

$$\begin{aligned} & \frac{d}{dr} G_\alpha(r) + \frac{\kappa}{r} G_\alpha(r) - (\epsilon_\alpha - V(r) + M^*(r)) F_\alpha(r) \\ & - \frac{f_v g_\omega}{2M^*(r)} \frac{d\omega_0(r)}{dr} G_\alpha(r) = 0, \end{aligned} \quad (13)$$

TABLE II. Results of infinite nuclear matter at the saturation point with $f_v = 0$. The energy per nucleon e_0 , the effective nucleon mass M^* , the value of incompressibility K_v , the scalar and vector potentials, S and V , are given in units of MeV; the saturation density ρ_0 is given in fm^{-3} .

e_0	M^*	K_v	S	V	ρ_0
-15.69	799.17	220.80	-138.72	83.10	0.15

$$\begin{aligned} & \frac{d}{dr} F_\alpha(r) - \frac{\kappa}{r} F_\alpha(r) + (\epsilon_\alpha - V(r) - M^*(r)) G_\alpha(r) \\ & + \frac{f_v g_\omega}{2M^*(r)} \frac{d\omega_0(r)}{dr} F_\alpha(r) = 0, \end{aligned} \quad (14)$$

with the effective nucleon mass $M^*(r)$ given by Eq. (2), and the vector potential $V(r)$ defined as

$$V(r) = g_\omega \omega_0(r) + \tau_\alpha g_\rho b_0(r) + \left(\frac{\tau_\alpha + 1}{2} \right) e A_0(r). \quad (15)$$

Here α is a reduced set of quantum numbers $\{n, \kappa, t_\alpha = \tau_\alpha/2\}$ [4], while $G_\alpha(r)$ and $F_\alpha(r)$ are, respectively, the radial parts of the upper and lower components of the solution to Dirac's equations for the nucleon

$$\psi_\alpha = \begin{pmatrix} i \frac{G_\alpha(r)}{r} \mathcal{Y}_{\kappa m} \\ \frac{F_\alpha(r)}{r} \mathcal{Y}_{-\kappa m} \end{pmatrix} \xi_{\tau_\alpha}, \quad (16)$$

where ξ_{τ_α} is a two-component isospinor with the isospin quantum number $\tau_\alpha = 1$ for the proton and $\tau_\alpha = -1$ for the neutron, and $\mathcal{Y}_{\kappa m}$, a spin spherical harmonic. The normalization condition for the Dirac wave function is

$$\int_0^\infty dr (|G_\alpha(r)|^2 + |F_\alpha(r)|^2) = 1. \quad (17)$$

The total energy of the system is given by

$$\begin{aligned} E = \sum_\alpha (2j_\alpha + 1) \epsilon_\alpha - \frac{1}{2} \int d^3r & \left[-m^*(r)^2 g_\sigma \rho_s(r) \phi(r) \right. \\ & + \frac{f_v g_\sigma g_\omega}{2M^2} \frac{d\omega_0(r)}{dr} \rho_t(r) + g_\omega \omega_0(r) \left(\rho(r) \right. \\ & + \frac{f_v}{2M^*(r)} \frac{d\rho_t(r)}{dr} + \frac{f_v g_\sigma}{2M^2} \frac{d\phi(r)}{dr} \rho_t(r) \left. \right) + g_\rho b_0(r) \rho_3(r) \\ & \left. + e A_0(r) \rho_p(r) \right]. \end{aligned} \quad (18)$$

TABLE III. Binding energy per nucleon B/A , rms charge radius r_c , and spin-orbit splittings of the nucleus ^{16}O as a function of the tensor coupling constant f_v . Values between parentheses are for protons, the others are for neutrons.

f_v	0	1	2	3	Expt.
B/A (MeV)	8.43	9.31	10.32	11.48	7.98
r_c (fm)	2.64	2.60	2.55	2.50	2.74
$\epsilon_{1p1/2} - \epsilon_{1p3/2}$ (MeV)	1.43(1.43)	2.84(2.83)	4.52(4.50)	6.52(6.49)	6.1(6.3)

Equations (4) to (14) are a closed set of coupled nonlinear differential equations, which can be solved with an iteration procedure.

The spin-orbit potential results from in a single particle Hamiltonian that acts on two-component wave functions. Now, we will adopt the method described in Ref. [12] to take out the spin-orbit part

$$h_{\text{ls}} = V_{\text{ls}} \vec{l} \cdot \vec{s}, \quad (19)$$

in which

$$V_{\text{ls}} = \frac{dV(r)}{dr} \frac{dS(r)}{dr} + \frac{f_v g_\omega}{m_{\text{eff}}(r) M^*(r) r} \frac{d\omega_0(r)}{dr} - \frac{f_v g_\omega \omega_0(r)}{m_{\text{eff}}(r) M^{*2}(r) r} \frac{dS(r)}{dr}, \quad (20)$$

with the vector potential $V(r)$ given by Eq. (15). The scalar potential $S(r)$ and $m_{\text{eff}}(r)$ are specified as

$$S(r) = -m^*(r) g_\sigma \phi(r), \quad (21)$$

$$m_{\text{eff}}(r) = M - \frac{1}{2}(V(r) - S(r)). \quad (22)$$

Similarly, the central potential in the MZM model is defined as [12]

$$V_0(r) = S(r) + V(r). \quad (23)$$

III. RESULTS AND DISCUSSIONS

The coupling constants $C_i^2 = (M^2/m_i^2)g_i^2$ ($i = \sigma, \omega$ and ρ) and the mass parameters for the MZM model are presented in Table I [11]. First, we investigated the properties of infi-

nite nuclear matter in the MZM model, the calculated results listed in Table II are quite reasonable for the nuclear matter in equilibrium. It is obvious that the obtained results of infinite nuclear matter with $f_v = 0$ in the MZM model are the same as those in the ZM model. Then we evaluated the properties of some nuclei ^{16}O , ^{40}Ca , ^{48}Ca , ^{90}Zr , and ^{208}Pb . Since the obtained results show that these two nuclei, ^{16}O and ^{208}Pb , are crucial, while the rest can be ignored, we will focus our discussion on these two nuclei. Our calculations on the binding energy per nucleon, the root-mean-square (rms) charge radius and the spin-orbit splittings of the nuclei ^{16}O and ^{208}Pb are presented in Tables III and IV. One can see from these tables that the rms charge radius r_c decreases slightly as f_v increases. In terms of the binding energy per nucleon this change operates in the opposite direction. It is clear that, with the increase in f_v value, the values of the spin-orbit splittings come close to those of the experimental data. In order to understand the physical source of these results, we show the variation of the spin-orbit potential with respect to the tensor coupling constant in Fig. 1. It is apparent that the spin-orbit potentials are strengthened with the increase in f_v value. As a result, the nucleons are more tightly bound as the tensor coupling gets stronger, so that the binding energy per nucleon increases and the rms charge radius decreases.

The scalar and vector potentials for the nuclei ^{16}O and ^{208}Pb are plotted in Fig. 2. In comparison with $f_v = 0$ (i.e., the ZM model), the vector potentials defined by Eq. (15) first increase and then decrease as f_v increases. However, the scalar potentials defined by Eq. (21) first decrease and then increase as f_v increases. The coordinates of the turning points are $r_t \approx 2.8$ fm for the small nucleus ^{16}O and $r_t \approx 6.7$ fm for the large nucleus ^{208}Pb . These turning radii are close to the average values predicted by the formula $r_t = 1.12A^{1/3}$ in the liquid-drop model. When compared, Figs. 2(a) and 2(b) indicate the potentials for the small nucleus ^{16}O are

TABLE IV. Binding energy per nucleon B/A , rms charge radius r_c , and spin-orbit splittings for the nucleus ^{208}Pb as a function of the tensor coupling constant f_v . Values between parentheses are for protons, the others are for neutrons.

f_v	0	1	2	3	Expt.
B/A (MeV)	7.83	8.07	8.31	8.57	7.87
r_c (fm)	5.55	5.53	5.51	5.50	5.50
$\epsilon_{2p1/2} - \epsilon_{2p3/2}$ (MeV)	0.22(0.23)	0.40(0.41)	0.61(0.61)	0.82(0.82)	0.5
$\epsilon_{2f7/2} - \epsilon_{2f5/2}$ (MeV)	0.52	0.94	1.39	1.89	1.8
$\epsilon_{3p1/2} - \epsilon_{3p3/2}$ (MeV)	0.19	0.34	0.50	0.67	0.9

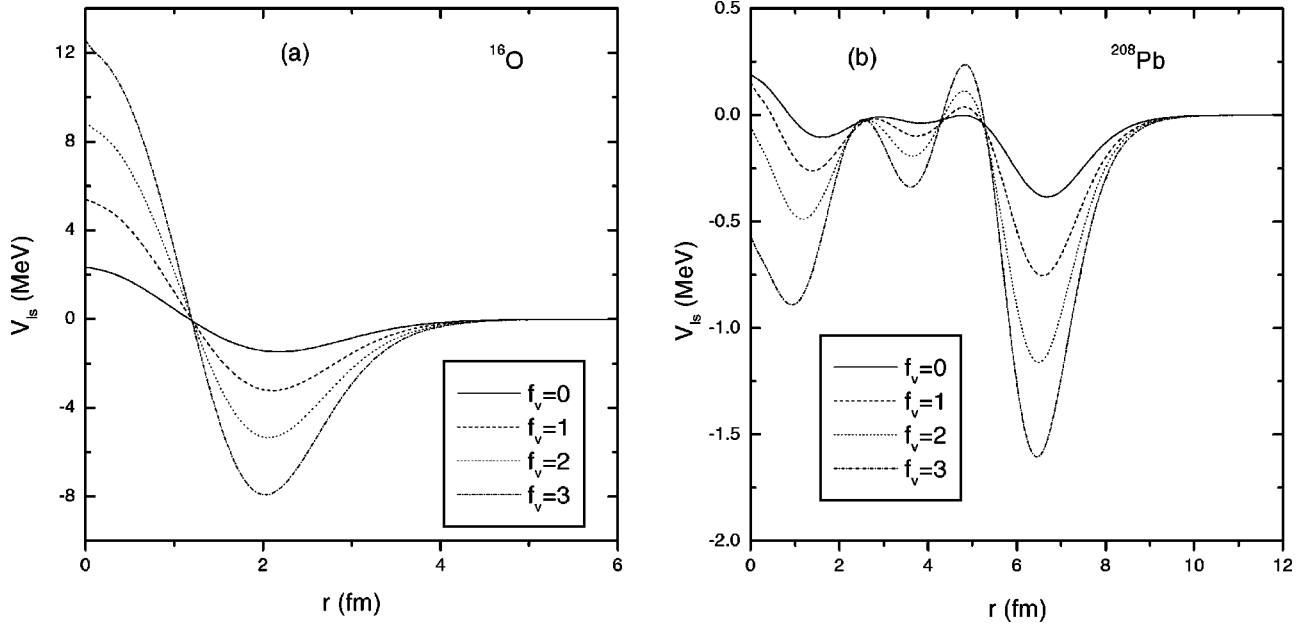


FIG. 1. The spin-orbit potential [defined by Eq. (20) in the text] as a function of the radial distance for $f_v=0, 1.0, 2.0,$ and 3.0 . (a) For the nucleus ^{16}O ; (b) for the nucleus ^{208}Pb .

more sensitive to the changes in f_v values.

Figure 3 shows the central potentials defined by Eq. (23) for ^{16}O and ^{208}Pb . For the small nucleus ^{16}O , in comparison with the curve of $f_v=0$, the central potential first goes deeper for $r \approx 0 - 2.8$ fm, then becomes shallower beyond $r_t \approx 2.8$ fm with the increase in f_v value. These results indicate the tensor force is generally attractive in the interior of the small nucleus ^{16}O and repulsive in the surface region ($r \geq r_t$). Although influenced by shell effects, the tensor force is mainly attractive in the interior of the large nucleus

^{208}Pb with $r \leq 6.7$ fm and repulsive in the surface region ($r \geq 6.7$ fm). As a result, the tensor force causes the tight binding of nucleons in the deep-lying occupied states and the loose binding of nucleons in the states close to the Fermi surface. This repulsive effect of the tensor force in the surface explicitly leads to that the nucleons in the states close to the Fermi surface are less bound with the increasing of f_v value, e.g., for the occupied states $1p_{1/2}$ in ^{16}O , and $3p_{1/2}$ (neutrons), $3s_{1/2}$ (protons), etc., in ^{208}Pb ; for the unoccupied states $1d_{5/2}$ and $2s_{1/2}$ in ^{16}O , and $2g_{9/2}, 1i_{11/2}$, etc., for neu-

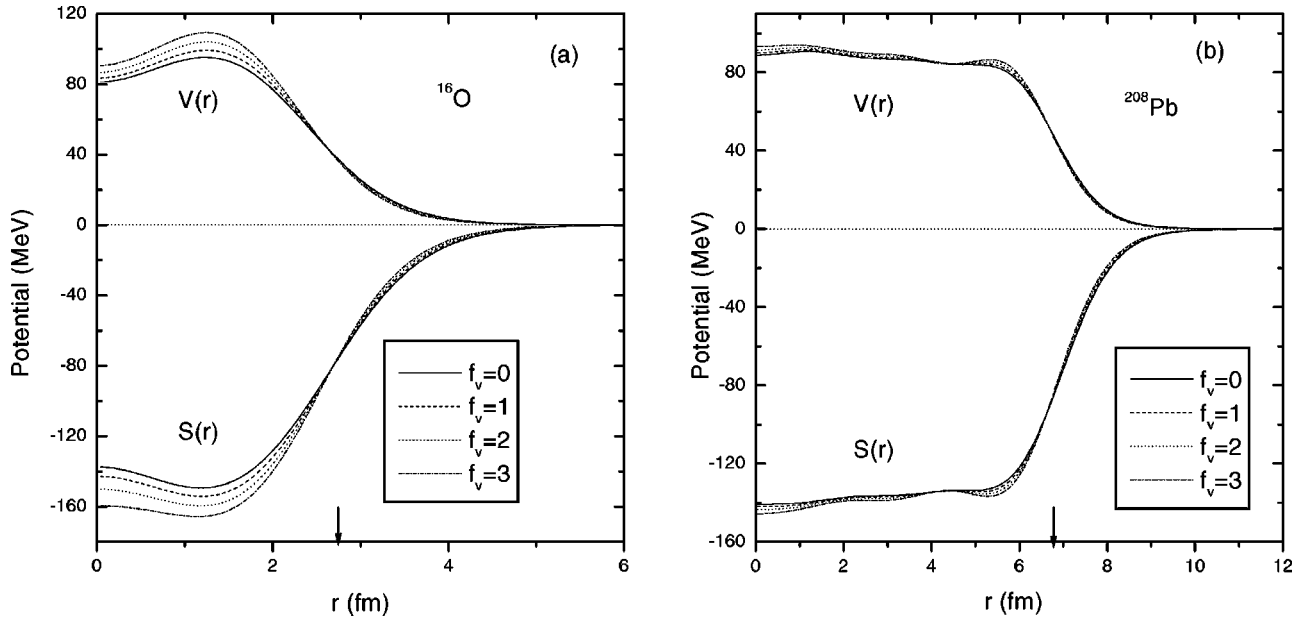


FIG. 2. The scalar and vector potentials [defined by Eqs. (21) and (15) in the text, respectively] as a function of the radial distance for $f_v=0, 1.0, 2.0,$ and 3.0 . (a) For the nucleus ^{16}O ; (b) for the nucleus ^{208}Pb . The short arrow at the transverse axis indicates the radial coordinate of the turning point (r_t).

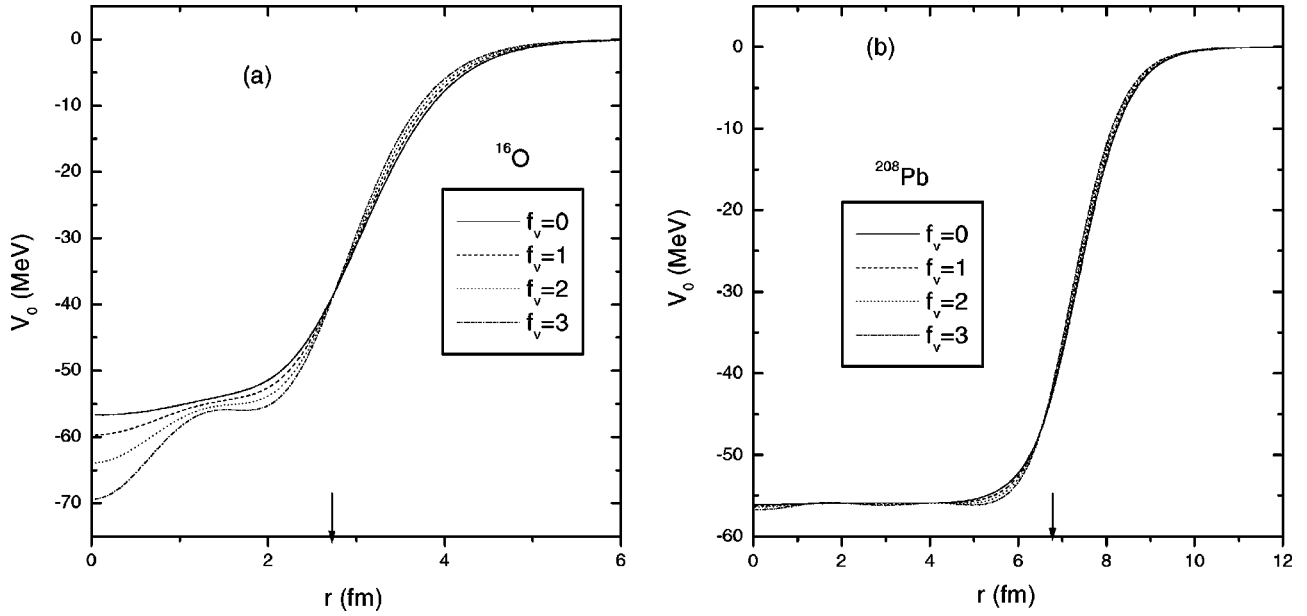


FIG. 3. The central potential [defined by Eq. (23) in the text] as a function of the radial distance for $f_v=0, 1.0, 2.0,$ and 3.0 . (a) For the nucleus ^{16}O ; (b) for the nucleus ^{208}Pb . The short arrow at the transverse axis indicates the radial coordinate of the turning point (r_t).

trons, and $1h_{9/2}, 2f_{7/2},$ etc., for protons in ^{208}Pb (see Figs. 5 and 6). One important point is that the tensor force is mainly proportional to the derivative of the ω -meson field with respect to the radial coordinate, and $\omega_0(r)$ changes slowly in the interior of the large nucleus. Therefore, the effect of the tensor force is relatively weak in the interior of the large nucleus ^{208}Pb , in comparison with that of the small nucleus ^{16}O .

The effective nucleon mass in the nuclei ^{16}O and ^{208}Pb is shown in Fig. 4. Since the effective nucleon mass is defined

by $M^*(r) = M + S(r)$, where the scalar potential $S(r)$ changes with f_v values as shown in Fig. 2. Clearly, it decreases in the region ($r \lesssim r_t$) and increases beyond the r_t with the increase in f_v value in comparison with $f_v=0$. For $f_v=0-3$, the average value of the effective nucleon mass at $r=0$ is about $M^*/M \approx 0.85$ for the nuclei ^{16}O and ^{208}Pb .

In Figs. 5 and 6, we show some occupied and unoccupied single particle energies in nuclei ^{16}O and ^{208}Pb as done in Ref. [12]. For the small nucleus ^{16}O in Fig. 5, neutrons (or protons) in the deep-lying occupied states of $1s_{1/2}$ and $1p_{3/2}$

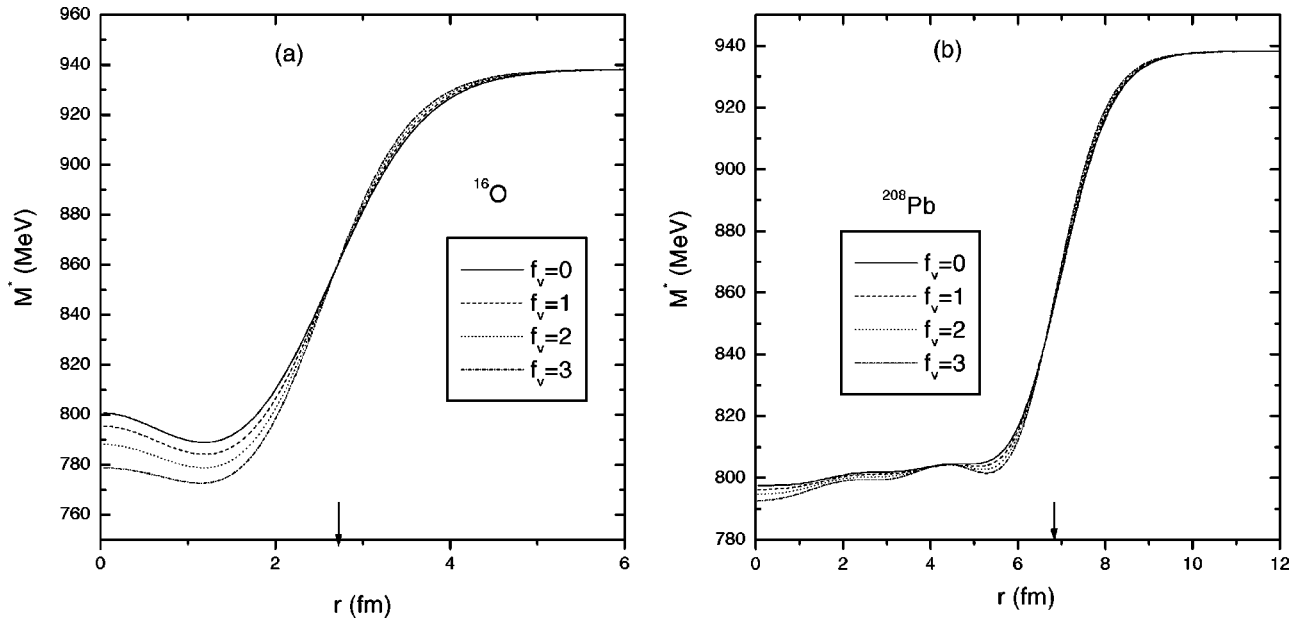


FIG. 4. The effective nucleon mass [defined by Eq. (2) in the text] in nuclei as a function of the radial distance for $f_v=0, 1.0, 2.0,$ and 3.0 . (a) For the nucleus ^{16}O ; (b) for the nucleus ^{208}Pb . The short arrow at the transverse axis indicates the radial coordinate of the turning point (r_t).

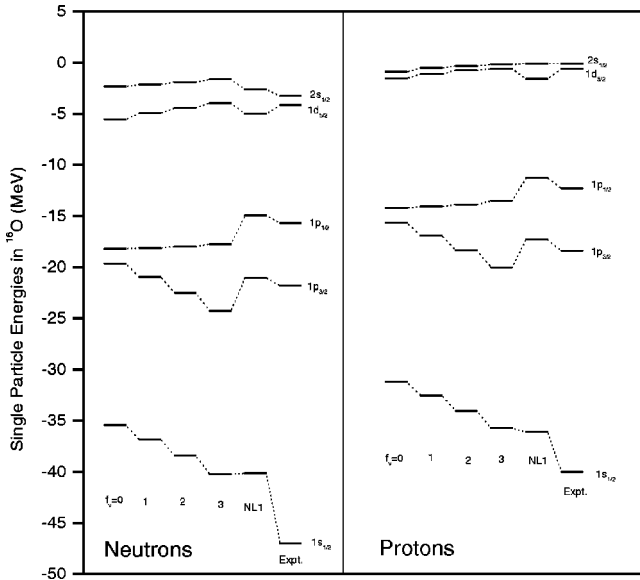


FIG. 5. The occupied and unoccupied single particle energies in ^{16}O . The experimental data are taken from Ref. [13].

are more bound with the increasing of f_v value. But neutrons (or protons) in the occupied states of $1p_{1/2}$, as well as in the unoccupied states of $1d_{5/2}$ and $2s_{1/2}$ tend to be less bound as f_v value increases. For comparison we also present the single particle energies in ^{16}O calculated by the nonlinear Walecka model with the parameter set NL1 and the experimental data [13], it is seen that the single particle energies given by the MZM model still deviate from those given by the nonlinear Walecka model and the experimental data. Similarly, for the large nucleus ^{208}Pb in Fig. 6, neutrons (or protons) in the deep-lying occupied states, e.g., $1s_{1/2}$, $1p_{3/2}$, and $1d_{5/2}$, are more bound, while nucleons in the occupied states close to the Fermi surface, e.g., $3p_{1/2}$ for neutrons and $3s_{1/2}$ for protons, as well as in the unoccupied states, e.g., $2g_{9/2}$, $1i_{11/2}$, etc., for neutrons, and $1h_{9/2}$, $2f_{7/2}$, etc., for protons, become less bound with the increasing of f_v value. From Figs. 5 and 6 it is also seen that the single particle energies (for occupied states) with the relative high total angular momentums, such as $1p_{3/2}$ in ^{16}O , $1i_{13/2}$, $1h_{11/2}$, $2d_{5/2}$, $1g_{9/2}$, $1f_{7/2}$, etc., for neutrons, and $1g_{9/2}$, $1f_{7/2}$, $1d_{5/2}$, and $1p_{3/2}$, etc., for protons in ^{208}Pb , become smaller with the increasing of f_v value. These results indicate that the nucleons in those occupied states are more bound as f_v increases. It is also self-evident that the single particle energies in the small nucleus ^{16}O are more sensitive to variations of f_v values.

IV. CONCLUSION

In summary, this paper is a study of the role the tensor coupling plays in the MZM model. The resultant calculations

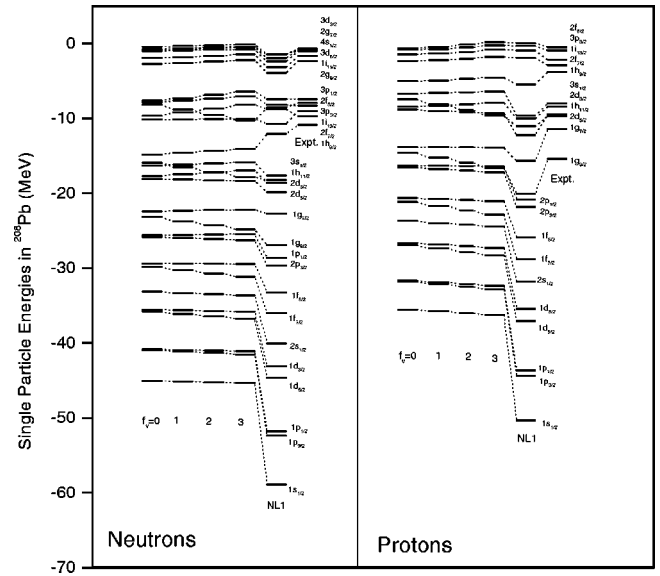


FIG. 6. The same as the Fig. 5 but for ^{208}Pb .

indicate that the tensor force can improve the agreement between the MZM model prediction and the experimental data for spin-orbit splittings. In addition, the tensor force has some influences on binding energies per nucleon, rms charge radii, and single particle energies as well. The study shows the tensor force is generally attractive in the interior of nuclei and repulsive in the surface region. As a result, nucleons are more tightly bound in the deep-lying states, and more loosely bound in the states close to the Fermi surface with the increasing of the tensor coupling. It is also shown that the nucleons in some occupied single particle states with the relative high total angular momentum become more bound as the tensor coupling constant increases. The value of the effective nucleon mass can remain large, while the spin-orbit splittings are improved if the tensor coupling is introduced in the MZM model. However, in comparison with the results given by the nonlinear Walecka model and the experimental data, it is shown that, besides the spin-orbit splittings improved in the MZM model, the inclusion of the tensor coupling seems not enough to improve the other shortcomings of the ZM model for finite nuclei.

ACKNOWLEDGMENTS

This project was supported in part by Major State Basic Research Developing Program with Grant No. G2000077400 and National Science Foundation of China. The authors thank Professor W. Perry for carefully reading and mending the manuscript.

- [1] J. Zimányi and S. Moszkowski, Phys. Rev. C **42**, 1416 (1990).
 [2] A. Delfino, C. T. Coelho, and M. Malheiro, Phys. Lett. B **345**, 361 (1995).
 [3] M. Malheiro, A. Delfino, and C. T. Coelho, Phys. Rev. C **58**,

426 (1998), and references therein.

- [4] B. D. Serot and J. D. Walecka, Adv. Nucl. Phys. **16**, 1 (1986); Int. J. Mod. Phys. E **6**, 515 (1997).
 [5] J. Németh, G. Papp, and H. Feldmeier, Nucl. Phys. **A647**, 107

- (1999).
- [6] W. Koepf, M. M. Sharma, and P. Ring, Nucl. Phys. **A533**, 95 (1991).
- [7] M. Chiapparini, A. Delfino, M. Malheiro, and A. Gattone, Z. Phys. A **357**, 47 (1997).
- [8] T. S. Biró and J. Zimányi, Phys. Lett. B **391**, 1 (1997).
- [9] R. K. Su, L. Li, and H. Q. Song, J. Phys. G **24**, 1735 (1998).
- [10] P. Wang, Z. W. Chong, R. K. Su, and P. K. N. Yu, Phys. Rev. C **59**, 928 (1999).
- [11] H. Guo, T. v Chossy, and W. Stocker, Phys. Rev. C **61**, 014307 (2000).
- [12] P. Ring, Prog. Part. Nucl. Phys. **37**, 193 (1996).
- [13] D. Vautherin and D.M. Brink, Phys. Rev. C **5**, 626 (1972).